Hindawi
Journal of Mathematics
Volume 2022, Article ID 5282980, 9 pages
https://doi.org/10.1155/2022/5282980

Research Article

Modelling and Simulation of Fluid Flow through a Circular Cylinder with High Reynolds Number: A COMSOL Multiphysics Study

Abid. A. Memon,[1] M. Asif Memon,[1,2] Kaleemullah Bhatti,[1] Kavikumar Jacob,[2] Thanin Sitthiwirattham,[3] Chanon Promsakon,[4] and Ilyas khan[5]

[1]*Department of Mathematics and Social Sciences, Sukkur IBA University, Sukkur 65200, Sindh, Pakistan*
[2]*Department of Mathematics and Statistics, Faculty of Applied Sciences and Technology, Universiti Tun Hussein Onn, Malaysia Batu Pahat 86400, Johar, Malaysia*
[3]*Mathematics Department, Faculty of Science and Technology, Suan Dusit University, Bangkok 10300, Thailand*
[4]*Department of Mathematics, Faculty of Applied Science, King Mongkut's University of Technology North Bangkok, Bangkok 10800, Thailand*
[5]*Department of Mathematics, College of Science Al-Zulfi, Majmaah University, Al-Majmaah 11952, Saudi Arabia*

Correspondence should be addressed to M. Asif Memon; asif-memon@iba-suk.edu.pk and Thanin Sitthiwirattham; thanin_sit@dusit.ac.th

Received 20 January 2022; Revised 6 April 2022; Accepted 20 April 2022; Published 19 May 2022

Academic Editor: Ram Jiwari

In this study, we intend to investigate the steady-state and laminar flow of a viscous fluid through a circular cylinder fixed between two parallel plates keeping the aspect ratio of 1 : 5 from cylinder radius to height of the channel. The two-dimensional, incompressible fluid flow problem has been simulated using COMSOL Multiphysics 5.4 which implements finite element's procedure. The flow pattern will be investigated by using the Reynolds number from 100 to 1000. The reattachment length formed at the back of the cylinder and drag force when the fluid comes to strike with the front surface of the cylinder is expressed in terms of Reynolds numbers. We propose to calculate the velocity and the pressure before and after the cylinder. For this purpose, two-line graphs before and after the cylinder will be drawn to check the impact of cylinder on both velocity and pressure. It was found that the percentage change in the velocity as well as pressure before to after the cylinder is changing their behaviours at $Re = 700$. The study is important because the empirical equations between the vortex's lengths formed along the cylinder using the linear regression process obtained in this study may be used for future implementation.

1. Introduction and Literature Review

When the fluid with any material properties comes to strike with any type of cylinders or obstacles of any shape, the formation of the recirculation [1–3] at the back of the obstacles often takes place. That complex movement is surrounded freely over the cylinders wrapped up by the flow [4, 5]. When such types of problems are under consideration, then one more thing could be discussed more rigorously, which is the drag force applied by these circular cylinders. There have been made several studies like observation by pressure-driven [6, 7] and other studies about lift force, i.e., the resistance to flow caused by friction factor of obstacles [8]. Various studies are available for the flow through the circular cylinders with different approaches [9–11] where mostly the lift and the drag forces are discussed within limits. The study of vortex shedding, velocity field, and pressure near the circular cylinder when the fluid comes into any region accepts a lot of importance in the field of computational fluid dynamics. Due to this fact, the fluid flow through the circular cylinder has a wide range of applications in the cooling towers, hot wire anemometers, nuclear

reactors, and fuel rods. Many researchers have put the light of their best efforts and used different numerical measures to analyze the fluid flow through a circular cylinder.

Golani and Dhiman [13] used the finite volume approach and discussed the fluid flow and heat transfer through a channel enclosed with the circular obstacle with a 50–180 range of the Reynolds number. They found that the lift and drag coefficients along shedding frequency are increasing with the increase in the Reynolds number. Rashidi et al. [14] studied the vortex structure and other flow parameters by the magnetic field flow through two side-by-side circular cylinders keeping spacing ratio of 1.6 to 4 with the help of the Stuart number from 0 to 5 and fixing the Reynolds number at 100. They discovered that the vortex formation can be seen near the cylinder, and the length of the vortex can be reduced when the magnetic field comes into action. Moreover, a critical Stuart number was found where the drag force through the cylinder is minimum. Faycal et al. [15] on applying the finite volume method through the multigrid acceleration investigated the two-sided lid-driven cavity induced by a cylindrical shape at the centre of the channel and tested the flow employing the Reynolds number ranging from 100 to 1500. It was found that when the Reynolds number is increasing up to 1500, the vortex is formed in the rear sides of the channel back to the cylinder. Elder [16], while observing airflow through the screen fitted in the middle of the rectangular channel, derived the solution known as asymptotic that gives the relationship between the numerically calculated stream-wise velocity to the analytically involving small inclination of the screen. Hauke and Hughes [17] derived the general approach of Galerkin's least-squares of the finite element method to solve the compressible and incompressible fluid flows problems. Memon et al. [18] used three screens in the rectangular channel to analyze the behaviour of the fluid flow exhausting the marketable tool COMSOL Multiphysics 5.4 and established that the drag force is decreasing by improving the angles of the screen turning into the clockwise direction. Memon et al. [19] used different values of the resistance coefficient of the screen to optimize the fluid velocity passing through the screen using the finite element-based software COMSOL Multiphysics 5.4. In this way, from [20–22], different researchers who used their different approaches were remaining busy to search out the flow behaviour through the different obstacles either circular or noncircular with different approaches. Considering the blood as the Casson fluid, magnetohydrodynamics impacts [23] were experienced in solving the fractional partial differential equation via the Laplace and finite Hankel transformation. The impacts testing revealed that using the fractional model brings tremendous changes as compared with those of the ordinary model, and the implications of the magnetic field decline the flow rate of the particles in the blood as well as magnetic particles. For the sake of comparison, an AB fractional derivative and the Caputo–Fabrizio derivative technique [24] were applied to the generalized Casson fluid in the case of free convection which contains the heat generation and first-order chemical reaction. It was concluded that with both approaches, the velocities obtained for the particles were identical in unit time and velocities differ with the enhancement of the time. In [25], the generalized Darcy model was used to check the impacts of anastomosis, vessel suppression, and obstructions on the total flow regime through the networks. With the use of similarity transformation [26], between the two parallel plates, an unsteady squeezed nanofluid was observed. The governing equation of mass and energy equations were used to simulate problem. A study was proposed [27] with a methodology based on the airway tree admittance to study the problem. This methodology was distinct from the traditional quantification, based on overall impedance using lump parameter models, and was applied to a matrix formed by admittances of each airway of the entire conducting part of the bronchial tree. The key finding of the study was to show how the position and intensity of local obstruction in an airway can affect the overall as well as regional ventilation which can lead to impaired gas exchange. A numerical approach was applied named scale-3 Haar wavelets [28] to study the impact of thermal radiation between the two parallel plates in the presence of magnetic effects. Convergence analysis of this study showed that the error could be minimized to zero by increasing the resolution level. Using the wavelet collocation procedure, an asymmetric channel was analyzed for its physical characteristics due to unsteady heat distribution and the spread of nanofluid flow [29]. The velocity and the temperature profiles were discussed in the terms of volume fraction, expansion ratio, and the Reynolds number. The characteristics of thermal transmission of the nanofluid flow through an asymmetric channel were discussed [30]. Three main algorithms were applied to the governing partial differential equations to develop the simulation in the rectangular channel. The velocity and temperature profiles were discussed in the terms of the Reynolds number and the volume fraction in addition to the expansion ratio.

In the current research article, the time-independent, Newtonian laminar flow through the circular cylinder will be discussed. The reattachment length of the two vortices formed at the back of the cylinder will be discussed in the terms of the Reynolds number. Finally, with the amplification of the linear regression procedure, the correlation known as empirical equations between the Reynolds number and reattachment length will be found. It has never been done in the previous research articles. The orientations of the velocity field magnitude and the pressure before and after the cylinders will be presented through the line graphs. The percentage changes in the average values of the velocity of the fluid and the pressure before and after the cylinder will be presented by the % change formula of increment or decrement in terms of the Reynolds number. Finally, the drag force at the front surface of the cylinder will be expressed in terms of the Reynolds. After doing this, we will make some conclusion points at the end.

2. Methodology

2.1. Geometrical Structure and Meshing of the Geometry. The schematic diagram of the pragmatic channel is shown in Figure 1. The length of the channel is 4 m, and the

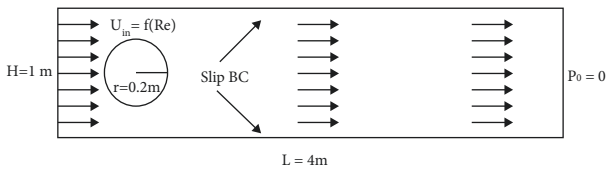

Figure 1: The schematic diagram of the channel.

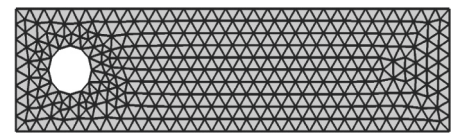

Figure 2: The irregular triangular meshes of the geometry.

height is 1 m. The aspect ratio from the radius of the cylinder to the height of the channel is taken as 1 : 5. An average velocity magnitude of U_{in} depending on the Reynolds number is introduced from the left entrance of the channel to start a fully developed flow whereas zero pressure is being considered at the passage of the channel. The upper and lower walls along with the boundaries of the circle are considered fixed with the implication of slip boundary to avoid viscous effect near the end of that boundary.

The channel under observation has meshed into small triangular elements. About 2880 elements are used to decompose the whole domain with minimum and average quality elements 0.633 and 0.9081, respectively, to get accurate results. Figure 2 depicts the meshing.

2.2. Governing Equations. Under consideration, the fluid flow problem is steady-state, Newtonian, incompressible, and laminar. The governing equations are elucidated by employing the boundary conditions through the use of commercial software COMSOL Multiphysics 5.4; see procedure in Figure 3. It has been many years that the system of partial differential equations created by the laws of conservation of momentum and mass has been serving to understand the complicated flow behaviour in the field of fluid dynamics. Let u and v be the components of the fluid velocity $\overrightarrow{V}$ than equations (1 and 2) are together called the Navier–Stokes equations:

$$(\overrightarrow{V}.\nabla)\overrightarrow{V} = -\frac{1}{\rho}\nabla p + \nabla^2\overrightarrow{V}, \tag{1}$$

$$\nabla.\overrightarrow{V} = 0. \tag{2}$$

Equations (1) are in vector form. We will write them in the component form with nondimensional form as follows [31]:

$$\begin{aligned} u\frac{\partial u}{\partial x} + v\frac{\partial u}{\partial y} &= -\frac{\partial p}{\partial x} + \frac{1}{\text{Re}}\left(\frac{\partial^2 u}{\partial x^2} + \frac{\partial^2 u}{\partial y^2}\right), \\ u\frac{\partial v}{\partial x} + v\frac{\partial v}{\partial y} &= -\frac{\partial p}{\partial x} + \frac{1}{\text{Re}}\left(\frac{\partial^2 v}{\partial x^2} + \frac{\partial^2 v}{\partial y^2}\right), \\ \frac{\partial u}{\partial x} + \frac{\partial v}{\partial y} &= 0. \end{aligned} \tag{3}$$

If ρ and μ are the density and viscosity of the air then in this problem, we have

$$\begin{aligned} \text{Re} &= \frac{\text{inertial force}}{\text{viscous force}}, \\ \text{Re} &= \frac{\rho U_{\text{in}} L}{\mu}. \end{aligned} \tag{4}$$

The upper and lower boundaries of the channel including the surface of the circular cylinder are considered as the wall in the problem. Moreover, to finish the viscous effects seen in the walls, we would apply the slip boundary conditions which are defined as follows:

$$u\frac{\partial v}{\partial y} + v\frac{\partial u}{\partial x} = 0, \tag{5}$$

where $\overrightarrow{n} = <\partial v/\partial y, \partial u/\partial x>$ is the normal vector to the velocity field $\overrightarrow{V} = <u, v>$.

To authenticate our numerical results, we match our result by the asymptotic solution resulting by the Elder [4] while perceiving the airflow pours through the screen inserted in the rectangular channel. The screen condition can be defined as follows:

$$\begin{aligned} [\rho\overrightarrow{V}\cdot\overrightarrow{n}]_-^+ &= 0, \\ \left[p - \overrightarrow{n}^T\overrightarrow{K}\overrightarrow{n} + \rho(\overrightarrow{V}\cdot\overrightarrow{n})^2\right]_-^+ &= -\frac{\kappa}{2}\rho_-\left(\overrightarrow{V}_-\cdot\overrightarrow{n}\right)^2, \end{aligned} \tag{6}$$

where

$$\begin{aligned} \overrightarrow{K} &= \mu\left(\nabla\overrightarrow{V} + (\nabla\overrightarrow{V})^T\right), \\ \overrightarrow{n}\times\overrightarrow{V}_+ &= \eta\left(\overrightarrow{n}\times\overrightarrow{V}_-\right), \end{aligned} \tag{7}$$

where *the "+" sign* shows the velocity upstream and "–" sign shows the velocity downstream. Elder [4] has derived the following relation where θ is the angle at which the screen is attached:

$$\frac{(-1)\left(1+\eta+k\cos^2\theta\right)}{(1-\eta)\tan\theta k\cos^2\theta} = \frac{2}{\pi}\log\left(\cot\left(\frac{\pi y}{2}\right)\right), \tag{8}$$

where k and η are resistance coefficient and refraction coefficient, respectively, and y is vertical length of the outlet. After achieving reliable results, we will determine our empirical equations by applying the linear regression process. If best fit linear (9) can be defined, then

$$y = a + bx, \tag{9}$$

where A and B can be determined by the formulae as follows:

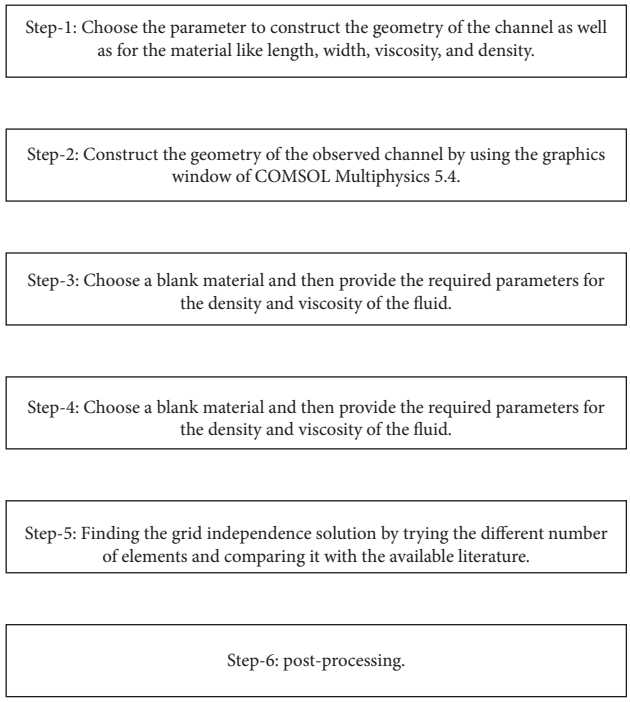

Figure 3: The working Wagon Wheel of COMSOL Multiphysics 5.4.

$$a = \frac{\sum (x_i - \overline{x})(y_i - \overline{y})}{\sum (x_i - \overline{x})^2}, \qquad b = \overline{y} - a\overline{x}. \tag{10}$$

Let α_i be the initial value of any parameter before cylinder and after passing through the cylinder becomes α_{i+1}, then mathematically we can determine the percentage increment or decrement by the formula as follows:

$$\%\ \text{increment or decrement} = \frac{\alpha_{i+1} - \alpha_i}{\alpha_i} \times 100. \tag{11}$$

Here, α_i are average values either presenting the average value of the velocity field magnitude or pressure before the cylinder. Also, α_{i+1} are presenting the average value of either the velocity magnitude or pressure after the cylinder. Formula (11) is often used to find the percentage change in the quantity from the initial state to the final state. We write formula (12) more clearly as

$$\%\ \text{change} = \frac{\text{final state} - \text{initial state}}{\text{initial state}} \times 100. \tag{12}$$

3. Validation and Comparison with the Asymptotic Solution

Before working to discuss the numerical results, we need to compare our results with the asymptotic solution delivered by Elder 1959 while perceiving the asymptotic solution through the rectangular passage fitting with the solid screen with inclination at the middle of the duct. Equation (9) defines the discovery of Elder where the left-hand term is planned through numerical approximation and the right hand is analytical observation. Figure 4 shows the stream-wise velocity calculated at the exit of the channel with screen boundary condition without cylinder, and Figure 5 is the result with the cylinder. It displays that our method is a good observation and comparable with the asymptotic solutions at low and high Reynolds numbers. In equation (14), the velocity field U is computed numerically by the finite element procedure. All other parameters are $U_{\text{in}} = f(\text{Re})$, $\kappa = 2.2$, $\eta = 0.78$, and $\theta = \pi/4$.

The same code is also checked for the validation by evaluating the drag coefficient for the hydrodynamics flow through the circular cylinder [32–34] (see Figure 6). It seems that the maximum percentage error in the accuracy of the results is ±2%.

4. Result and Discussion

The numerical results through the finite element method via COMSOL Multiphysics 5.4 are obtained to observe the Newtonian, laminar flow of the air in the presence of a circular cylinder [35, 36] with the help of the nondimensional Reynolds number from 100 to 1000. Here, we are going to discuss the Reattachment length formed at the end of the cylinder and viewed through the streamline pattern of the velocity field, drag force applied by the cylinder. When any type of fluid is passing across the cylinder, the average flow rate (average velocity) of the fluid is increasing and average pressure is decreasing. To observe the phenomenon, we find the velocity magnitude as well as pressure before and after the cylinder by drawing two lines L_1 and L_2 before and after the cylinder, respectively, as shown in Figure 7.

4.1. Reattachment Length and Drag Force. In the field of thermodynamics, especially for the production of heat exchangers, often obstacles are used in the channel to create vortices having a certain reattachment length. The reattachment lengths are responsible for slowing down the velocity field magnitude and increasing the temperature distribution over the domain. The streamlined configuration of the velocity field is visualized in Figure 8. It is shown that at Re = 100, there was no reattachment seen at the boundary of the circular cylinder. However, at Re = 200, it is visualized that two vortices or reattachment lengths are formed at the right front of the cylinder. Also, by increasing the Reynolds number from 200 to 1000, the length of the two vortices is increasing constantly with the increase in the Reynolds number. At Re = 1000 in Figure 6, the two big vortices of equal size can be seen. We determine that the reattachment length or length of the vortices is the function of the Reynolds number and increases with the increase in the Reynolds number (see Figure 9(a)). Using the linear regression process, we can determine the empirical equation that can express the length of the vortices in terms of the Reynolds number and that can be used for future exercises.

$$\text{Vortex length} = 0.00086\text{Re} + 0.0364. \tag{13}$$

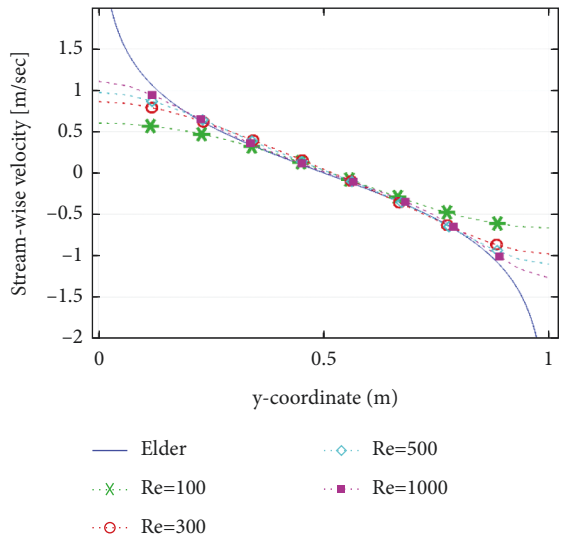

Figure 4: Stream-wise velocity without screen boundary conditions.

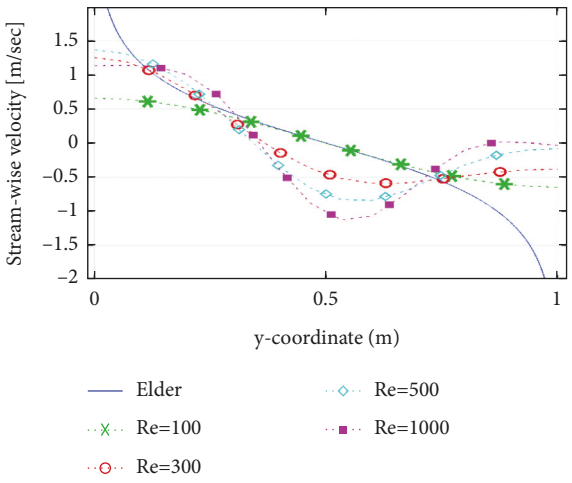

Figure 5: Stream-wise velocity with screen boundary conditions.

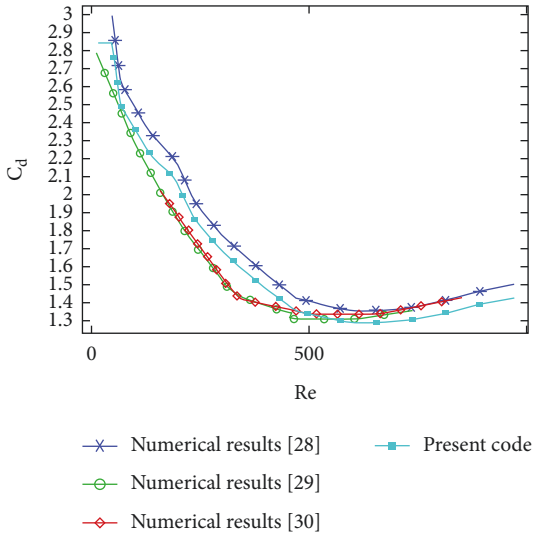

Figure 6: The validation of the present code with other numerical approaches [32–34].

Fluid when to enter into the region and to strike with the surface of the cylinder with a force has two components such as lift and drag forces. Basically, the drag force F_d is given by the formula as follows:

$$F_d = \frac{1}{2} C_d \rho u A, \tag{14}$$

where C_d, A, and u are the drag coefficient, area, and velocity of the fluid while the fluid is striking with the front surface of the cylinder.

We can determine the drag force in COMSOL Multiphysics 5.4 by integrating the total stress in the y-direction over the front of the cylinder. The graph through Figure 9(b) shows the drag force on the front surface of the circular cylinder with increasing Reynolds number. The drag force possesses a direct relationship with that of the Reynolds number and reveals the message that with the increase in the Reynolds number, the drag force is also increasing.

Figure 7: Line L_1 and L_2 before and after the cylinder.

4.2. Velocity Field and Pressure. In this stage, we are going to describe the orientation of the velocity field as well as pressure before and after the circular cylinder. For this purpose, we draw two lines before and after the circle which is equidistant from the circle and to determine the velocity magnitude as well as pressure by the numerical procedure through COMSOL Multiphysics 5.4. In Figure 10, we found the velocity magnitude in line 1 before the circle and line 2

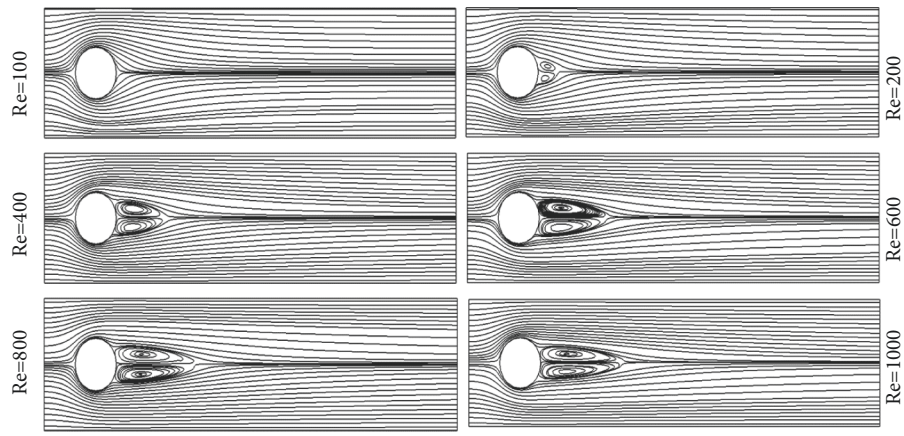

Figure 8: Streamline pattern of the velocity field for $100 < Re < 1000$.

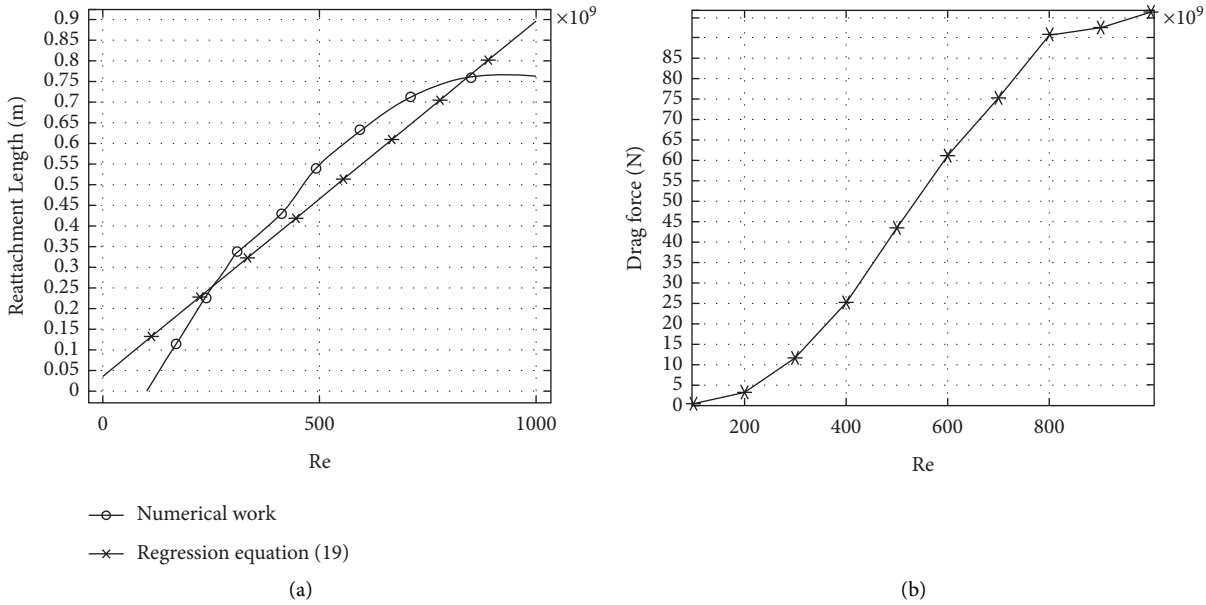

Figure 9: (a) Reattachment length via numerical work and regression equation and (b) drag force at the front of the cylinder.

after the circle, and it is deducted that the flow rate in the middle of the channel is minimum. It is showing that after striking off the fluid with the circular obstacle, the fluid losses it is power and slows down and therefore vortex can be seen there.

Figures 11(a) and 11(b) represent the percentage change in the flow rate of fluid before to after the cylinder, respectively. It is clear that the change in average velocity V_{av} is increasing with the increase in the Reynolds number up to $Re = 700$ and then it is decreasing till $Re = 1000$. Likely to the velocity field, the pressure is also reducing gradually when the fluid is passing through the cylinder. In Figure 12, the pressure at lines 1 and 2 is calculated for $Re = 100$, 500, and 1000 which shows that the pressure at the middle of the channel is maximum. It is also clear that with the increase in the Reynolds number, the difference in the pressure is also increasing. So, while the fluid across the cylinder is losing it is power for a particular Reynolds number, the pressure is reducing and becomes negative. In Figure 12(b), we calculate the percentage increments in the average pressure before to after the cylinder, and the graph shows that with the increase in the Reynolds number, increment is going to decrease up to $Re = 700$ and it is minimum at $Re = 700$.

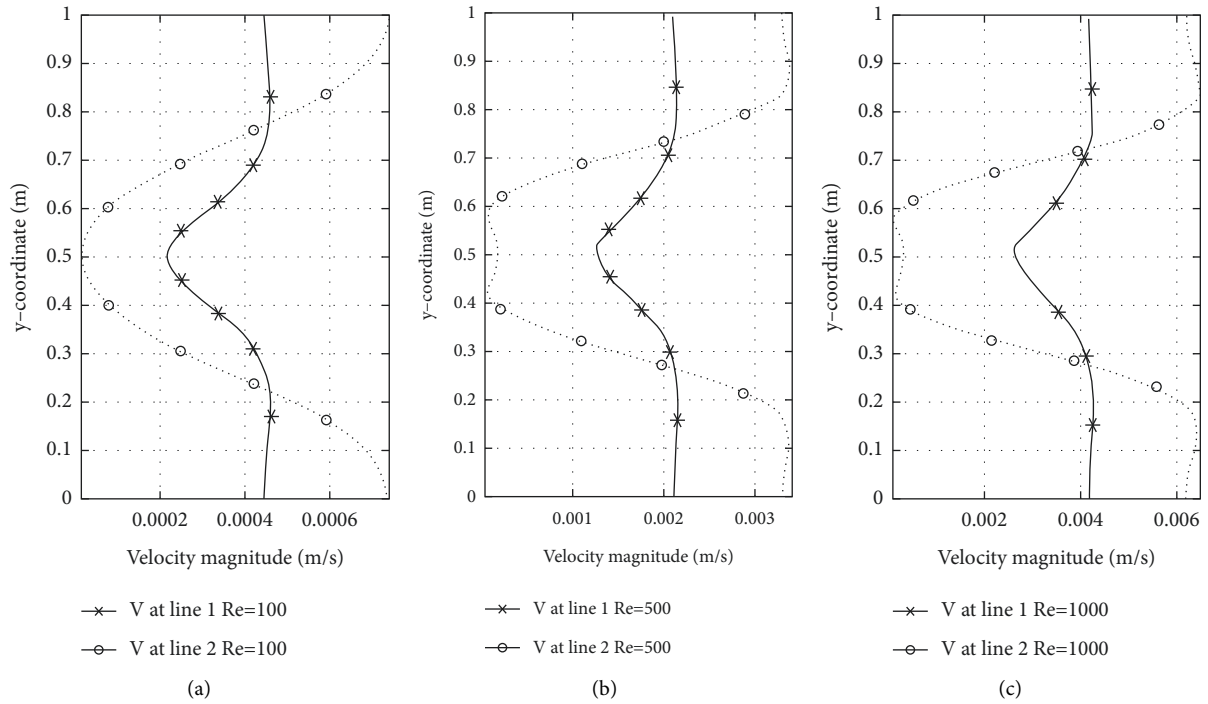

Figure 10: Velocity magnitude of the fluid before and after the cylinder at (a) Re = 100, (b) Re = 500, and (c) Re = 1000.

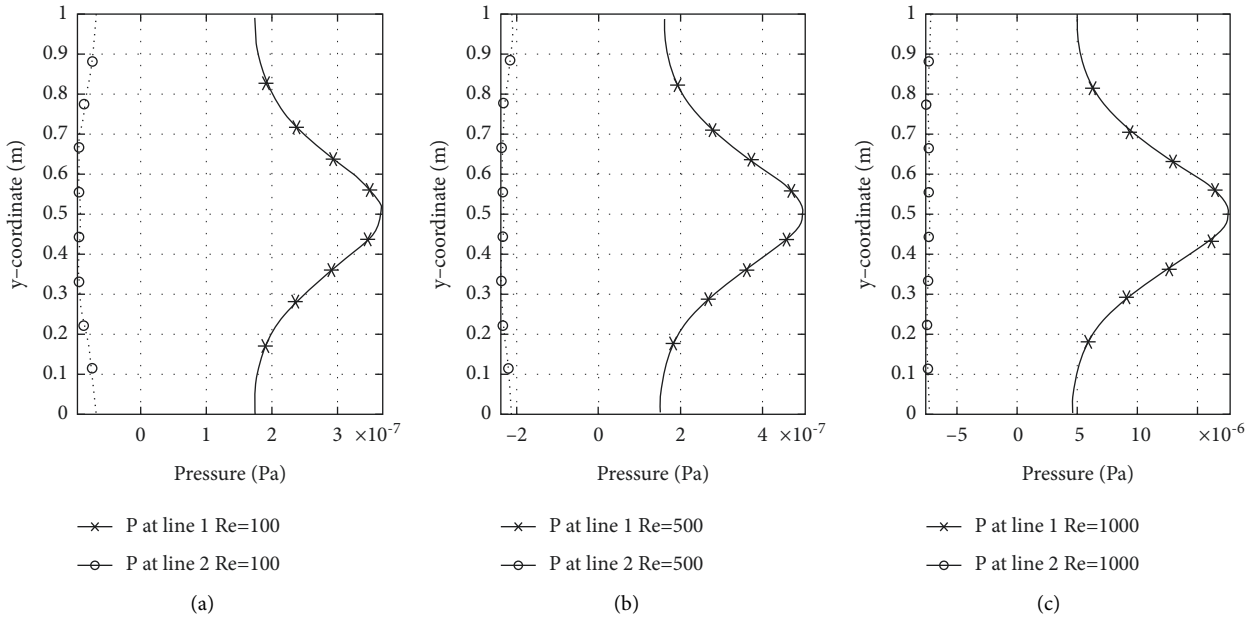

Figure 11: Pressure (Pa) of the fluid before and after the cylinder: (a) Re = 100, (b) Re = 500, and (c) Re = 1000.

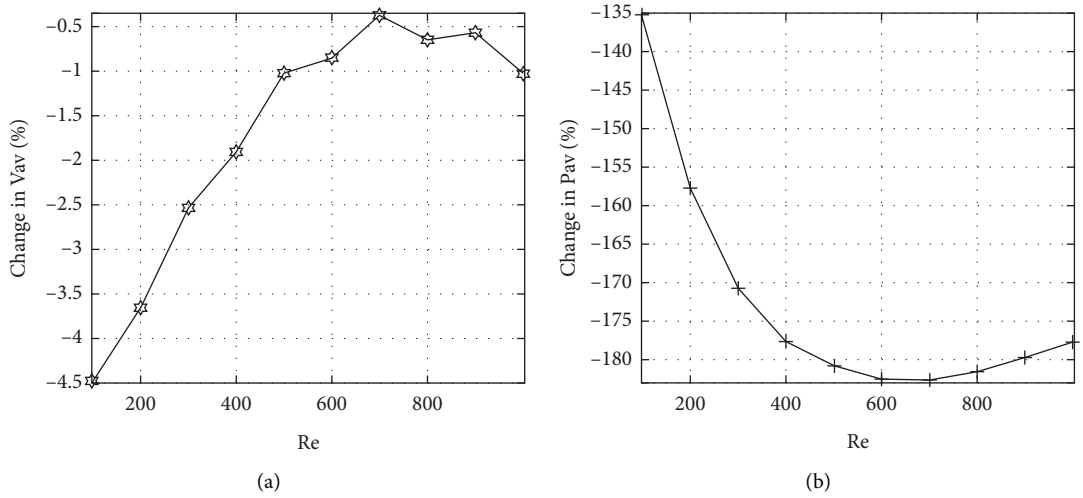

Figure 12: Percentage change before and after cylinder (a) Average velocity (b) Average pressure.

5. Conclusion

The finite element method procedure has been applied to discretize the momentum and continuity equations to get the numerical solution for incompressible fluid flow through the rectangular channel embedded by circular cylinder using the Reynolds number from 100 to 1000 keeping the aspect ratio of 1 : 5 from the diameter of the cylinder to the height of the channel. The vortex length formed at front of the cylinder, drag force related to the Reynolds number, velocity field orientation, and pressure before and after have been presented through streamlined patterns and graphs. The numerical results achieved are compared with the asymptomatic solution provided by the Elder [4]. From our problem, we can describe the following points:[36], [37–39]

(1) The drag force on the front face of the circular cylinder is increasing with the increase in the Reynolds number.

(2) In the steady-state flow, the two vortexes can be seen at the end of the boundary of the cylinder, and the length of that vortices is the function of the Reynolds number and increases with the increase in the Reynolds number. An empirical equation related to the vortex length of the Reynolds number was represented by using linear regression.

(3) Velocity magnitude is losing power while passing through the cylinder, and the increment in the average velocity is increasing with the increase in the Reynolds number up to $\mathrm{Re} = 700$ and then decreasing.

(4) The pressure before and after the cylinder is decreasing; hence, the increment of the average pressure before to after cylinder is decreasing up to 700 and then increasing unless $\mathrm{Re} = 1000$.

Data Availability

No data were used for this research.

Conflicts of Interest

The authors declare that there are no conflicts of interest regarding the publication of this paper.

Acknowledgments

This research was funded by King Mongkut's University of Technology North Bangkok Contract no. KMUTNB-64-KNOW-48.

References

[1] S. Taneda, "Experimental investigation of the wake behind a sphere at low Reynolds numbers," *Journal of the Physical Society of Japan*, vol. 11, no. 10, pp. 1104–1108, 1956.

[2] M. Nishioka and H. Sato, "Measurements of velocity distributions in the wake of a circular cylinder at low Reynolds numbers," *Journal of Fluid Mechanics*, vol. 65, no. 1, pp. 97–112, 1974.

[3] C. Norberg, "An experimental investigation of the flow around a circular cylinder: influence of aspect ratio," *Journal of Fluid Mechanics*, vol. 258, pp. 287–316, 1994.

[4] G. Subramanian and D. L. Koch, "Inertial effects on the transfer of heat or mass from neutrally buoyant spheres in a steady linear velocity field," *Physics of Fluids*, vol. 18, no. 7, Article ID 073302, 2006.

[5] P. M. Kulkarni and J. F. Morris, "Suspension properties at finite Reynolds number from simulated shear flow," *Physics of Fluids*, vol. 20, no. 4, Article ID 040602, 2008.

[6] G. Segré and A. Silberberg, "Behaviour of macroscopic rigid spheres in Poiseuille flow Part 1. Determination of local concentration by statistical analysis of particle passages through crossed light beams," *Journal of Fluid Mechanics*, vol. 14, no. 1, pp. 115–135, 1962.

[7] G. Segré and A. Silberberg, "Behaviour of macroscopic rigid spheres in Poiseuille flow Part 2. Experimental results and interpretation," *Journal of Fluid Mechanics*, vol. 14, no. 1, pp. 136–157, 1962.

[8] P. G. Saffman, "The lift on a small sphere in a slow shear flow," *Journal of Fluid Mechanics*, vol. 22, no. 2, pp. 385–400, 1965.

[9] E. S. Asmolov, "The inertial lift on a spherical particle in a plane Poiseuille flow at large channel Reynolds number," *Journal of Fluid Mechanics*, vol. 381, pp. 63–87, 1999.

[10] J.-P. Matas, J. F. Morris, and É. Guazzelli, "Lateral force on a rigid sphere in large-inertia laminar pipe flow," *Journal of Fluid Mechanics*, vol. 621, pp. 59–67, 2009.

[11] M. P. Howard, *Structure and dynamics in colloid-polymer mixtures out of equilibrium*, Princeton University, Princeton, NJ, USA, PhD Diss, 2018.

[12] R. Golani and A. Dhiman, "Fluid flow and heat transfer across a circular cylinder in the unsteady flow regime," *International Journal of Engineering Sciences*, vol. 3, no. 3, pp. 8–19, 2004.

[13] S. Rashidi, M. Bovand, and J. Abolfazli Esfahani, "Application of magnetohydrodynamics for suppressing the fluctuations in the unsteady flow around two side-by-side circular obstacles," *The European Physical Journal Plus*, vol. 131, no. 12, p. 423, 2016.

[14] F. Hammami, B. Souayeh, N. Ben-Cheikh, and B. Ben-Beya, "Computational analysis of fluid flow due to a two-sided lid driven cavity with a circular cylinder," *Computers & Fluids*, vol. 156, pp. 317–328, 2017.

[15] J. W. Elder, "Steady flow through non-uniform gauzes of arbitrary shape," *Journal of Fluid Mechanics*, vol. 5, no. 3, pp. 355–368, 1959.

[16] G. Hauke and T. J. R. Hughes, "A unified approach to compressible and incompressible flows," *Computer Methods in Applied Mechanics and Engineering*, vol. 113, no. 3-4, pp. 389–395, 1994.

[17] A. A. Memon, H. Shaikh, and A. Ali Memon, "Finite element's analysis of fluid flow through the rectangular channel with inclined screens settled at angles," in *2019 2nd International Conference on Computing, Mathematics and Engineering Technologies (iCoMET)*, pp. 1–5, IEEE, 2019.

[18] A. A. Memon, "Analysis of optimum velocity and pressure of the air flow through the screens with the help of resistance coefficient," *Sukkur IBA Journal of Computing and Mathematical Sciences*, vol. 3, no. 1, pp. 51–57, 2019.

[19] X. Zhang, H. Huang, Y. Zhang, and H. Wang, "Influence of a magnetic obstacle on forced convection in a three-dimensional duct with a circular cylinder," *Journal of Heat Transfer*, vol. 138, no. 1, Article ID 011703, 2016.

[20] T. GulerBengusu, K. Yapici, and Y. Uludag, "Flow characterization of viscoelastic fluids around square obstacle," *Periodica Polytechnica - Chemical Engineering*, vol. 63, no. 1, pp. 246–257, 2019.

[21] A. Kumar, A. Dhiman, and L. Baranyi, "CFD analysis of power-law fluid flow and heat transfer around a confined semi-circular cylinder," *International Journal of Heat and Mass Transfer*, vol. 82, pp. 159–169, 2015.

[22] C. A. Klettner, I. Eames, and J. C. R. Hunt, "The effect of an unsteady flow incident on an array of circular cylinders," *Journal of Fluid Mechanics*, vol. 872, pp. 560–593, 2019.

[23] F. Ali, N. A. Sheikh, I. Khan, and M. Saqib, "Magnetic field effect on blood flow of Casson fluid in axisymmetric cylindrical tube: a fractional model," *Journal of Magnetism and Magnetic Materials*, vol. 423, pp. 327–336, 2017.

[24] N. A. Sheikh, F. Ali, M. Saqib et al., "Comparison and analysis of the Atangana-Baleanu and Caputo-Fabrizio fractional derivatives for generalized Casson fluid model with heat generation and chemical reaction," *Results in Physics*, vol. 7, pp. 789–800, 2017.

[25] A. M. Torres Rojas, A. Meza Romero, I. Pagonabarraga, R. D. M. Travasso, and E. Corvera Poiré, "Obstructions in vascular networks: relation between network morphology and blood supply," *PLoS One*, vol. 10, no. 6, Article ID e0128111, 2015.

[26] R. C. Mittal and S. Pandit, "Numerical simulation of unsteady squeezing nanofluid and heat flow between two parallel plates using wavelets," *International Journal of Thermal Sciences*, vol. 118, pp. 410–422, 2017.

[27] B. Soni and A. F. Miguel, "Gas flow in occluded respiratory tree: a new matrix-based approach," *Journal of Fluids Engineering*, vol. 144, no. 7, Article ID 071207, 2022.

[28] S. Pandit and S. Sharma, "Sensitivity analysis of emerging parameters in the presence of thermal radiation on magnetohydrodynamic nanofluids via wavelets," *Engineering with Computers*, pp. 1–10, 2021.

[29] S. Pandit and S. Sharma, "Wavelet strategy for flow and heat transfer in CNT-water based fluid with asymmetric variable rectangular porous channel," *Engineering with Computers*, pp. 1–11, 2020.

[30] A. M. Alqahtani and J. Ram, "Wavelet operational matrices and Lagrange interpolation differential quadrature-based numerical algorithms for simulation of nanofluid in porous channel," *Journal of Mathematics*, vol. 2022, 2022.

[31] B. Soni, A. F. Miguel, and A K. Nayak, "A mathematical analysis for constructal design of tree flow networks under unsteady flow," *Proceedings of the Royal Society A*, vol. 476, p. 2240, Article ID 20200377, 2020.

[32] R. D. Henderson, "Details of the drag curve near the onset of vortex shedding," *Physics of Fluids*, vol. 7, no. 9, pp. 2102–2104, 1995.

[33] O. Posdziech and R. Grundmann, "Numerical simulation of the flow around an infinitely long circular cylinder in the transition regime," *Theoretical and Computational Fluid Dynamics*, vol. 15, no. 2, pp. 121–141, 2001.

[34] M. Sahin and R. G. Owens, "A numerical investigation of wall effects up to high blockage ratios on two-dimensional flow past a confined circular cylinder," *Physics of Fluids*, vol. 16, no. 5, pp. 1305–1320, 2004.

[35] M. Sato and T. Kobayashi, "A fundamental study of the flow past a circular cylinder using Abaqus/CFD," in *2012 SIMULIA Community Conference*, RI, USA, May 2012.

[36] I. Khan, A. A. Memon, M. Asif Memon et al., "Finite element least square technique for Newtonian fluid flow through a semicircular cylinder of recirculating region via COMSOL multiphysics," *Journal of Mathematics*, vol. 2022, 2020.

[37] B. F. Armaly, F. Durst, J. C. F. Pereira, and B. Schönung, "Experimental and theoretical investigation of backward-facing step flow," *Journal of Fluid Mechanics*, vol. 127, no. –1, pp. 473–496, 1983.

[38] M. R. Ahmed and F. Talama, "Flow characteristics and local heat transfer rates for a heated circular cylinder in a crossflow of air," *International Journal of Fluid Mechanics Research*, vol. 35, p. 1, 2008.

[39] A. A. Memon, H.-U. Shaikh, B. A. Shah, M. A. Soomro, A. G. Shaikh, and A. H. Sheikh, "Modeling and simulation of Newtonian fluid flow through two-dimensional backward-facing step channel with finite Element's technique," *Indian Journal of science and technology*, vol. 12, no. 32, pp. 1–6, 2019.